



Fluid Hyperthermia and Ultrasonic Studies on Nickel Ferrite Magnetic Nanoparticles

V. BEULA SHANTHI AMMANI AMMAL^{1,*} and N. JOHN JEBARATHINAM^{2,*}

¹Department of Physics, Jerusalem College of Engineering, Narayanapuram, Chennai-600100, India

²Department of Chemistry, Jerusalem College of Engineering, Narayanapuram, Chennai-600100, India

*Corresponding author: E-mail: johnjebarithnam@jerusalemengg.ac.in

Received: 14 January 2023;

Accepted: 3 May 2023;

Published online: 27 May 2023;

AJC-21262

Superparamagnetic nickel ferrite (NiFe₂O₄) nanoparticles were synthesized by low temperature hydrothermal method using EDTA as templating agent. The synthesized nanoparticles were characterized by FTIR, XRD, FESEM and TEM analysis. The XRD analysis shows the presence of cubic spinel phase with crystallite size of 26.42 nm. The morphology analyzed by FESEM and TEM techniques indicate the presence of cubical shape particles having average particle size of 28.44 nm with no agglomeration. The VSM analysis gives “S” shape curve with zero coercivity and saturation magnetization (Ms) of 30 emu/g indicating the presence of small magnetic particles exhibiting the superparamagnetic behaviour. Nickel ferrite nanofluids were prepared by mixing carrier fluid water with varying amounts of nickel ferrite nanopowder. Zeta potential measurements of dilute solution of nickel ferrite show the formation of stable nickel ferrite nanofluids. Hyperthermia and ultrasonic studies were carried out on various concentrations of nickel ferrite nanofluids. The SAR values and ultrasonic parameters were calculated. Less concentrated nickel ferrite nanofluids quickly attain threshold hyperthermia temperature of 43 °C when exposed to lower applied AC magnetic field of range 5 mT to 20 mT. Ultrasonic studies show at lower concentrations nickel nanoparticles interact with carrier fluid water through cohesive forces mainly hydrogen bonding and keep the particles in an isolated state there by continue to exhibit superparamagnetic characteristics. At higher concentrations, particle-particle interaction predominantly occurs leading to increase in particle size beyond 30 nm, so that the magnetic characteristics of nickel ferrite nanoparticles changes from superparamagnetic to ferromagnetic nature. At low concentrations induction heating occurs through Neel and Brownian relaxation mechanism whereas at high concentrations hysteresis loss mechanism operate to attain the threshold temperature of 43 °C.

Keywords: Nanoparticles, Superparamagnetic, Hydrothermal, Hyperthermia, Nanofluids, Ultrasonic velocity.

INTRODUCTION

Metal nanoparticles found significant place in various biomedical applications [1-4] and have a substantial hope in the fields of cancer therapy [5], gene therapy [6], drug delivery systems [7-9] anti-inflammatory effects in allergic disease [10], therapy for allergic asthma [11], molecular imaging [12,13], Magnetic resonance contrast agents [14] and antimicrobial activities [15]. As cancer is a challenging health problem and the cancer therapeutics currently have the lowest clinical trial success rate, large areas of scientific research being dedicated to fight against cancer [16]. Gold nanoparticles are widely tested for anticancer treatments. Gold nanoparticles loaded with doxorubicin are used for cancer treatment [17] and the efficiency of gold nanoparticles conjugated with cellular uptake peptides for destroying lymphoma cells specifically [18]. However, there

are limitations in the usage of nanoparticles for the selective targeting and destroying of cancer cells.

The biggest problem is that before the nanoparticles reach the desired target cells they have to pass through a variety of barriers, such as blood vessels and the blood-brain barrier which leads to several neurodegenerative disorders. Magnetic nanoparticles are found to be best suited to overcome this targeting limitations [19]. Obaidat *et al.* [20] demonstrated that the magnetic anisotropy of the magnetic nanoparticle is an important factor for medical treatments, which help to direct the magnetic nanoparticles to a target site using an external magnetic field. Among various magnetic nanomaterials, spinel ferrites are widely used as soft magnetic materials [21] and have much scope in the field of biomedical applications, such as tumour treatment by hyperthermia. Among the spinel ferrites, nickel ferrites have emerged as wonder magnetic material used in

numerous fields [22] including magnetic fluid hyperthermia applications due to the release of thermal energy out of hysteresis loss or Neel/Brownian relaxations, which can be utilized for heating of specific tissue/organs for cancer treatment [23]. Another interesting feature associated with nickel ferrite that it exhibits superparamagnetic characteristics when the particle size is less than 30 nm [24].

Superparamagnetic nanomaterials generate rapid heating with high specific absorption rate (SAR) in the presence of small alternating magnetic field and do not retain any magnetism after removal of the magnetic field. This behaviour is an important property for heating of specific cells in the magnetic fluid hyperthermia cancer treatment without causing any harm to the healthy cells. Bae *et al.* [25] studied the biocompatibility of NiFe₂O₄ nanoparticles and reported that uncoated NiFe₂O₄ magnetic nanoparticles have a high value of cell survival rate (85%). In their work, the cytotoxicity of NiFe₂O₄ magnetic nanoparticles was also evaluated in agars with various pH values (pH = 7 normal cell and pH level = 6 tumour cell). These reports of non-cytotoxicity and superparamagnetic characteristic of nickel ferrite nanoparticle provide scope for using it for magnetic fluid hyperthermia cancer treatment to selectively destroy tumour cells. In present investigation, the superparamagnetic nickel ferrite nanoparticles were synthesized by hydrothermal method and nickel ferrite nanofluids prepared using water as carrier fluid were utilized for hyperthermia analysis. However, since heat is generated due to the application of alternating magnetic field during hyperthermia analysis the generated heat may facilitate agglomeration of particles due to particle-particle interactions leading to formation of small clusters with large particle size. As the particle size is important for nickel ferrite to impart super paramagnetic property it is required to know an insight into the nature of interactions existing in the nickel ferrite nanofluids with rise of temperature in the presence of an applied magnetic field

The ultrasonic studies on nanofluids are extensively used to predict the nature of interactions such as particle-fluid and particle-particle interactions through the measurement of ultrasonic parameters like ultrasonic velocity and acoustic impedance [26,27]. Generally, the particle-particle interaction in nanofluids leads to the formation of clusters. Hence, a thorough investigation of hyperthermia and ultrasonic analysis on various concentrations of nickel ferrite nanofluids prepared using water as carrier fluid will help to identify the efficiency and suitability of nickel ferrite nanofluids for magnetic fluid hyperthermia applications.

EXPERIMENTAL

Synthesis of nickel ferrite nanoparticles: The chloride salts *e.g.* NiCl₂·6H₂O and FeCl₂·6H₂O used for the synthesis of NiFe₂O₄ were of AnalaR grade purchased from Merck India.

The purchased chemicals were used as such without any further purification. Calculated amount of NiCl₂·6H₂O and FeCl₂·6H₂O in the molar ratio 1:2 dissolved in 50 mL of deionized water was added to 50 mL of a solution containing 0.5 g of disodium salt of ethylenediamine tetraacetic acid (EDTA) with constant stirring by magnetic stirrer followed by the addition of 4.4 molar NaOH solution dropwise till the pH reached to 11-12. The precipitate produced was stirred for another 3 h at room temperature. Then, the precipitate was transferred into an autoclave (23 mL capacity with Teflon lining) and kept at 160 °C for 15 h in an air oven. The precipitate obtained was centrifuged and washed with distilled water and ethanol. The wet precipitate was then dried at 110 °C for 3 h in an air oven.

Characterization: The synthesized nickel ferrite nanoparticles were characterized by FTIR, XRD, FESEM and TEM analysis. The Fourier transform infrared (FTIR) was performed by KBr tablet method in the range 4000-250 cm⁻¹, in a BRUKER model IFS 66 V FTIR spectrometer. The FTIR spectra of the synthesized spinel ferrites are given in Fig. 1a. Two distinct vibrational absorption bands were observed at 480 and 602 cm⁻¹ which are characteristic to octahedral metal-oxygen and tetrahedral metal-oxygen bonds, respectively [28].

Powder X-ray diffraction (XRD) patterns were measured by using RICH-SIEFERT 3000-TT diffractometer employing CuKα radiation. The XRD pattern of the synthesized nickel ferrite shown in Fig. 1b exhibit typical reflections of (220), (311), (222), (400), (422), (511) and (440) planes, which are indications of the presence of the cubic spinel structure. All the diffraction peaks were matched well with the reported values (JCPDS file No. 10-0325). There are no peaks obtained for capping agent EDTA indicating that the nanocrystalline ferrites obtained *via* this method consists of ultrapure phase without impurities.

The average crystallite diameter was estimated by the Scherrer's equation using the peak broadening (FWHM) of the most intense peak (3 1 1). Cation distribution in octahedral and tetrahedral sites is determined by X-ray intensity calculation method [29]. NiFe₂O₄ exhibit inverse spinel structure with all bivalent Ni²⁺ present at tetrahedral sites along with half of trivalent Fe³⁺ ions and the remaining half of the trivalent Fe³⁺ ions present at the octahedral sites. Lattice constant was calculated from the *d*-spacing obtained from XRD patterns. The calculated crystal parameters and cation distribution are given in Table-1.

The morphology of the synthesized nickel ferrite was investigated by FESEM analysis performed by FEI Nova-Nano SEM-600 (The Netherlands) spectroscopy. FESEM micrograph for NiFe₂O₄ and corresponding EDAX spectra are shown in Fig. 1c. It shows diamond-cube like particles with average size of 28.44 nm with no agglomeration. No impurities are observed in the EDAX spectrum, once again confirming that the synthe-

TABLE-1
CRYSTAL PARAMETERS AND CATION DISTRIBUTION IN NICKEL FERRITE

Spinel ferrite	Lattice constant (a) (Å)	Volume of unit cell (a ³) (Å) ³	Average crystallite size (nm)	Cation distribution at	
				Tetrahedral site	Octahedral site
Nickel ferrite	8.36	584.27	26.42	Fe ³⁺	Ni ²⁺ , Fe ³⁺

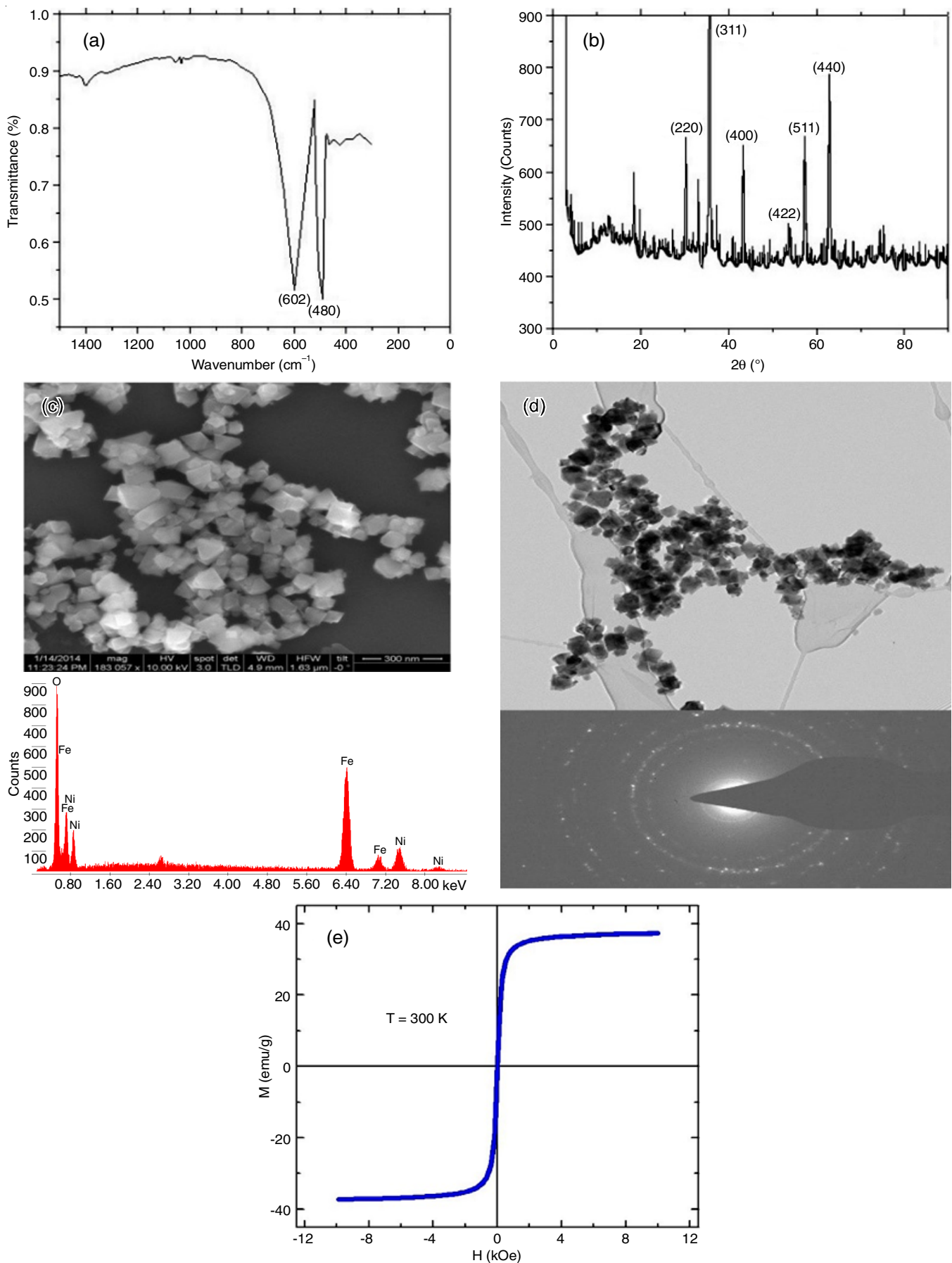


Fig. 1. Characterization of nickel ferrite (a) FTIR (b) XRD (c) FESEM (d) TEM (e) VSM

sized nickel ferrite is pure in nature. The morphology of the synthesized nanospinel ferrites was also studied by TEM techniques using FEI Tecnai G2-F20 scanning transmission electron microscope. The TEM images and selected area electron diffraction pattern (SAED) taken on one of the crystals for NiFe_2O_4 is shown in Fig. 1d. The image indicates presence of cubical shape particles along with few particles with incomplete octahedron shape. The particles are well isolated and no agglomeration is observed. The selected area electron diffraction (SAED) pattern shows good crystalline nature of single-phase nano- NiFe_2O_4 .

The average particle size was found to be much smaller than the value 170 nm reported by Wang *et al.* [30] who have synthesized NiFe_2O_4 by solvothermal method. Lassoued *et al.* [31] synthesized NiFe_2O_4 by coprecipitation method with average particle size of 35 nm but observed particle agglomeration. It is clearly observed that EDTA assisted low temperature hydrothermal synthesis of NiFe_2O_4 produces nanoparticles of much smaller size (less than 30 nm) without undergoing particle agglomeration. Magnetic measurements were performed by vibrating sample magnetometer (VSM) at room temperature using quantum design SQUID vibrating sample magnetometer. Hysteresis loop for NiFe_2O_4 (Fig. 1e) is typical for soft magnetic materials and the “S” shape of the curve with the zero coercivity and saturation magnetization $M_s = 30 \text{ emu/g}$ indicate the presence of small magnetic particles exhibiting superparamagnetic behaviour.

Preparation of nickel ferrite nanofluids: Two-step preparation process [32] was used for the synthesis of nickel ferrite nanofluids by mixing carrier fluid water with the synthesized nickel ferrite nano powder. The stability of nickel ferrite nanofluids prepared using water as carrier fluid was confirmed by zeta potential measurements. A dilute solution of nickel ferrite in water (0.01 wt.%) was prepared by dispersing 0.01 g of nickel ferrite nanoparticles in 100 mL of deionized water followed by sonication for 30 min. Zeta potential was measured using NanoZS (Malvern UK) employing a 532 nm laser at a back-scattering angle of 173° . The measured value of zeta potential (Fig. 2) was found to be -57 mV.

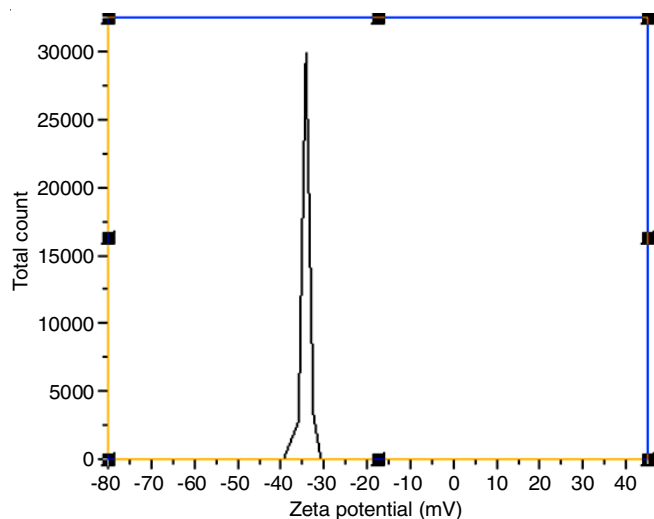


Fig. 2. Zeta potential 0.01 wt.% nickel ferrite nanofluids

As colloidal suspensions having more than 30 mV are stable, aqueous nickel ferrite nanoparticles in water form stable nanofluids. In present investigation, nickel ferrite nanofluids of different concentrations (0.2, 0.4, 0.6, 0.8 and 1.0 wt.%) were prepared by dispersing specific amount of the synthesized nickel ferrite nanoparticles in 100 mL of deionized water followed by sonication for 4 h.

RESULTS AND DISCUSSION

Fluid hyperthermia studies: Hyperthermia studies were carried out for all the prepared samples under various AC magnetic fields ranging from 15 to 50 mT using EASY HEAT laboratory induction power supply at 250 KHz. During the experiment the coil was cooled to room temperature using a closed loop circulating water system. The prepared nanofluids (1 mL) were placed at the center of coil and various magnetic fields are applied. The saturation temperatures attained under each field were measured for all the prepared nickel ferrite nanofluids of concentrations 0.2, 0.4, 0.6, 0.8 and 1.0 wt.%. It was found that significant induction heating is observed even in the presence of a lower AC magnetic field of 5 mT. Hence, the applied AC magnetic field is fixed at 5 mT and increased up to 40 mT to investigate the heating ability of various nickel ferrite nanofluids to attain the targeted hyperthermia temperature of 43°C .

The variation of induction heating with time of all the prepared nanofluids (0.2, 0.4, 0.6, 0.8 and 1.0 wt.%) under various AC magnetic fields are shown in Fig. 3a-e. The saturation temperature obtained for all the nickel ferrite nanofluids are given in Table-2. It is observed (Fig. 3a) that the induction heating of 0.2 wt.% increases rapidly with time up to 12 min and beyond 12 min the temperature almost remains constant. Fig. 3b obtained for 0.4 wt.% of nickel ferrite nanofluids show gradual increase of temperature with time for 5 mT and 10 mT applied magnetic fields and attain the saturation temperature of 44°C and 50°C , respectively in 12 min. On applying higher magnetic field of 15 mT and 20 mT the temperature increases rapidly and attain the saturation temperature of 52°C and 52.4°C , respectively in 6 min. The induction heating of nickel ferrite nanofluids of concentrations 0.6 wt.% (Fig. 3c) indicates a rapid increase of temperature with time and attain saturation in 9 min under all applied magnetic fields. Significantly different behaviour (Fig. 3d,e) of induction heating is observed for 0.8 and 1.0 wt.% nickel ferrite nanofluid samples. The temperature increases very slowly with time and it take 21 min to attain a constant temperature which is less than 35°C . As the saturation temperature is much less to the threshold hyperthermia temperature of 43°C , studies were carried out on these samples with higher applied magnetic field of 30 mT and 40 mT. It was found that the temperature increases gradually and attain saturation in 35 min (Fig. 3d,e). The saturation temperature is found to be 43°C and 44°C for 0.8 wt.% and 1.0 wt.% samples, respectively.

Effect of nanofluid concentration and applied magnetic field on saturation temperature: The effect of concentration of nickel ferrite nanofluid on saturation temperature is shown in Fig. 4a. The saturation temperature increases with increase

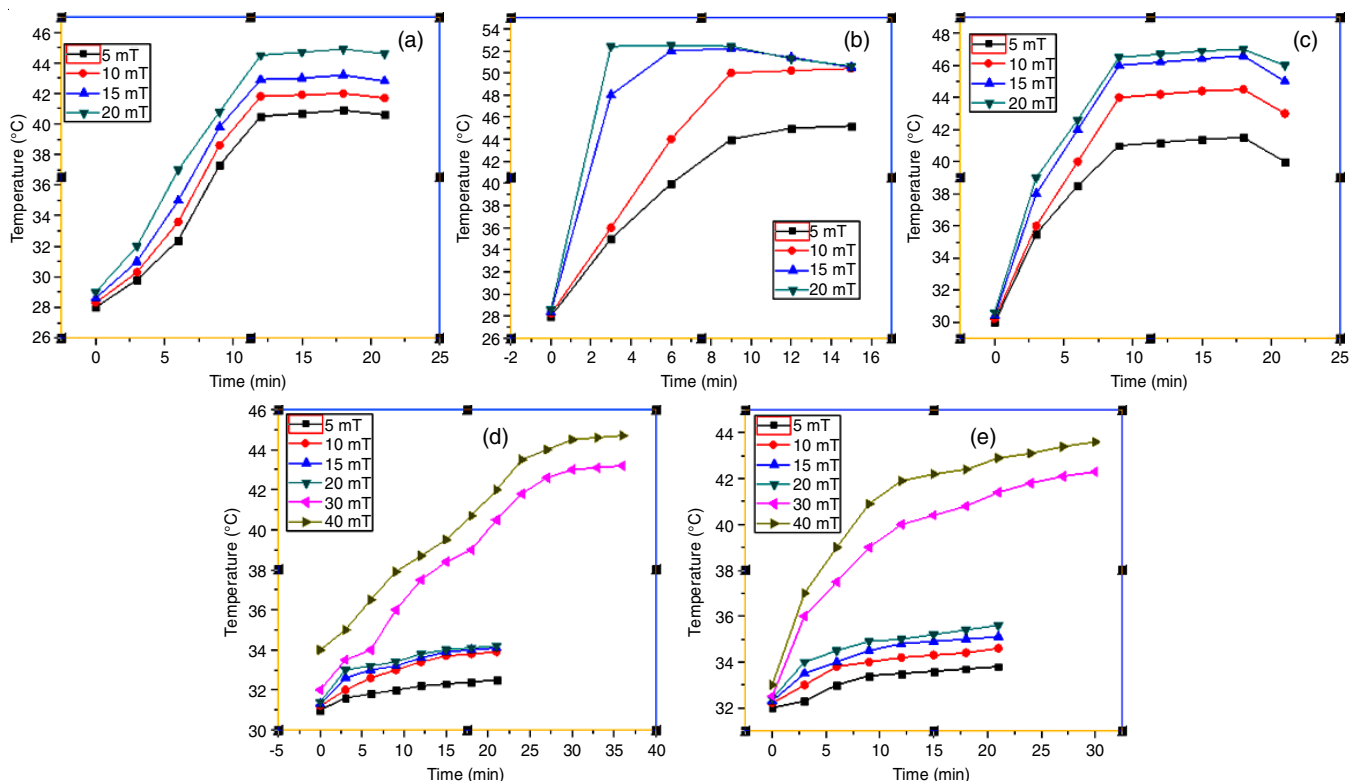


Fig. 3. Attainment of saturation temperature (a) 0.2 wt.% (b) 0.4 wt.% (c) 0.6 wt.% (d) 0.8 wt.% (e) 1.0 wt.%

TABLE-2
SATURATION TEMPERATURE AND SPECIFIC ABSORPTION RATE (SAR) OF NICKEL FERRITE

Field (mT)	0.20%		0.40%		0.60%		0.80%		1.00%	
	SAT (°C)	SAR (W/g)								
5	40.5	105.2	41	117.3	41	130.2	32	37.6	33	36.8
10	41.8	112.8	44	132.8	50	161.2	33.4	41.8	34	39.5
15	42.9	116.6	46	150.5	52	180.3	33.6	41.9	34.5	40.6
20	44.5	125.1	46.5	152.7	52.4	181.5	34	42.2	35	41
30	-	43	118.5	41	115.2	-	-	-	-	-
40	-	44	122.6	42	116	-	-	-	-	-

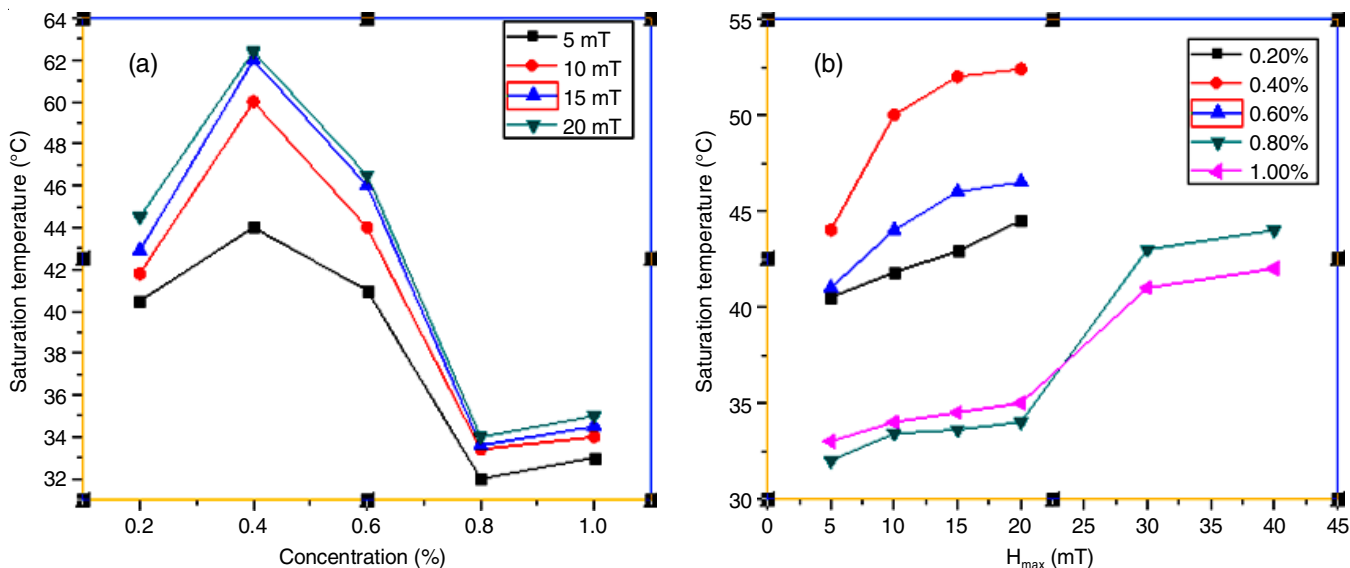


Fig. 4. (a) Effect of nanofluid concentration and (b) effect of applied AC magnetic field on saturation temperatures

of concentration up to 0.4 wt.% and beyond which it decreases under all magnetic fields. The same trend is observed under all applied magnetic fields (5 mT to 20 mT). The threshold hyperthermia temperature of 43 °C is attained even in the presence of 5 mT for 0.4 wt.% sample. Whereas in the case of 0.2 wt.% and 0.6 wt.% samples, it is required to apply a magnetic field of 15 mT and 10 mT, respectively to reach 43 °C. On the other hand, samples with 0.8 wt.% and 1.0 wt.% nickel ferrite nanoparticles show very low saturation temperatures of less than 35 °C. The influence of applied magnetic field on the saturation temperature is depicted in Fig. 4b. It shows increase of saturation temperature with increase of applied AC magnetic field for all nanofluid concentrations. A unique behaviour is observed for sample with 0.4 wt.% nickel ferrite nanoparticles, which has all the saturation temperatures more than 43 °C under all applied magnetic fields. An increase of more than 15 mT is required for 0.2 wt.% and 10 mT for 0.6 wt.% samples to attain 43 °C. Nickel ferrite nanofluids with 0.8 and 1.0 wt.% also show increase in saturation temperature with increase in magnetic field but the increase is small and not reaching 43 °C till 20 mT of applied field. Hence, a higher magnetic field is applied to identify whether any further rise in saturation temperature occur. It is found that the saturation temperature is increased beyond 30 mT significantly and attain the targeted temperature of 43 °C (Fig. 4b).

Effect of nanofluid concentration and applied magnetic field on specific absorption rate (SAR): Thermal property of magnetic nanofluids is characterized by SAR and defined as magnetic field energy that is spent for heating per second per unit mass(W/g). The specific absorption rate or SAR is a valuable parameter, which indicate how much energy is converted into heat per unit time and per unit mass of the magnetic nanoparticles. The SAR value is dependent on the frequency and amplitude of the alternating magnetic field (AMF). It is an important value for nanofluids, particularly when they are used for fluid hyperthermia treatment. If the SAR value is higher than more heat will be produced by the magnetic nanoparticles. In other words, the magnetic nanofluids with higher SAR values will require

less power of magnetic field to attain the threshold temperature of 43 °C for fluid hyperthermia applications.

Specific absorptin rate (SAR) values were calculated using the following equation:

$$\text{SAR} = C \left(\frac{\Delta T}{\Delta t} \right) \left(\frac{1}{m} \right)$$

where C is the nanofluid's heat capacity, $(\Delta T/\Delta t)$ characterizes the temperature change with time, m is a mass of nickel ferrite in nanofluid. The calculated SAR values for the nickel ferrite nanofluids at various concentrations under various external magnetic fields are given in Table-2 along with saturation temperatures.

The effect of nanofluid concentration and applied magnetic field on SAR are shown in Fig. 5a-b, respectively which appear to be same as that of effect of nanofluid concentration and applied magnetic field on saturation temperature given in Fig. 4a-b.

The values of SAR increases with increase of concentration up to 0.4 wt.% and beyond which it decreases under all magnetic fields. The same trend is observed under all the applied magnetic fields (5 mT to 20 mT). The actual SAR values (Table-2) found on 0.4 wt.% is considerably higher (130.2 to 181.5 W/g) compare to the SAR values obtained on all other nanofluids. It clearly demonstrates the unique behaviour of this sample in hyperthermia analysis. Similarly, the nanofluids with 0.8 and 1.0 wt.% of nickel ferrite particles show significantly small SAR under applied magnetic fields of 5 mT to 20 mT. However, on applying higher magnetic field SAR values are increased considerably. Self heating of magnetic nanofluids is mainly due to three mechanisms namely hysteresis loss, Neel relaxation and Brownian relaxations. The nature of magnetic property associated with the material and particle size determine the actual mechanism of self-heating. Nanomaterials possessing ferromagnetic behaviour with hysteresis loop of high coercivity are generating heat by hysteresis loss when placed in an alternating magnetic field [33]. But superparamagnetic material has zero remanence absorb power using Brownian and Neel relaxations and these relaxations generate more heat compared to conventional ferro/ferri-magnetic particles exhibiting

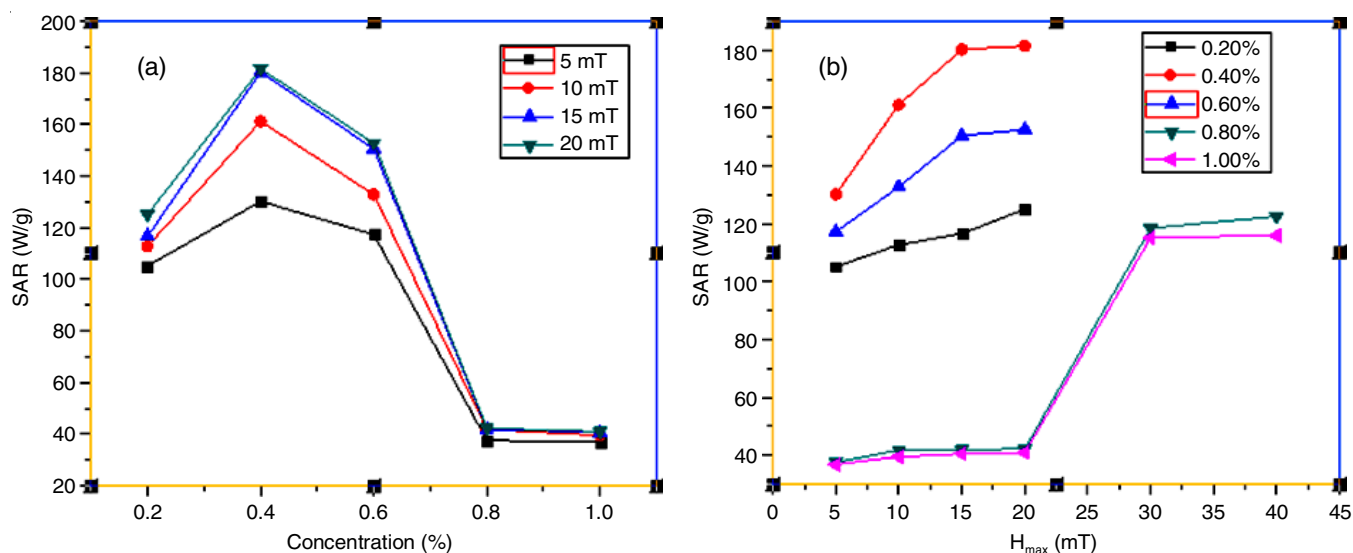


Fig. 5. (a) Effect of nanofluid concentration and (b) effect of magnetic field on SAR

hysteresis losses [34]. Nickel ferrite nanoparticle used in the present studies show superparamagnetic behaviour (Fig. 1). Hence, the nickel ferrite nanoparticles can transform the energy of magnetic field into heat only by Neel relaxation and Brownian relaxation mechanisms.

The experimental results of hyperthermia analysis are presented in Fig. 4a,b, Fig. 5a,b and Table-2 demonstrated that nanofluid concentration up to 0.6 wt.% generate heat rapidly and attain 43 °C under applied AC magnetic field less than 20 mT. This observation may be attributed to Neel and Brownian relaxation for magnetic energy absorption and transformation to heat energy. The higher value of SAR for these samples also confirm the above fact. Specifically nickel nanofluid with 0.4 wt.% found to show high SAR values and saturation temperatures at all magnetic fields. This observation indicates relatively higher efficiency of 0.4 wt.% sample compare to all other nickel ferrite nanofluid samples studied. The lower values of SAR and saturation temperatures up to 20 mT for 0.8 and 1.0 wt.% samples indicate the absence of Neel and Brownian mechanisms to generate induction heating. However, increase of SAR and saturation temperatures when these are placed under higher magnetic field of 30 mT and 40 mT can be explained only if hysteresis loss mechanism occur under this condition. As the nickel ferrite nanoparticles used in the present investigation possess superparamagnetic behaviour, as such there is no possibility of hysteresis loss mechanism for induction heating. Nejadi & Zabihi [24] studied the preparation and magnetic properties of nanosize nickel ferrite particles using hydrothermal method, established that when the diameter of particles is less than 30 nm, nickel ferrite shows the character of superparamagnetism and above this size it changes to ferromagnetism with hysteresis loop of significant coercivity. The VSM analysis of the synthesized nickel ferrite used in the present investigation show the superparamagnetic behaviour as the average particle size is below the critical size of 30 nm. However, when the concentration of nickel ferrite nanoparticles increased above 0.6 wt.% in the carrier fluid water it seems agglomeration occurs making particle size greater than 30 nm and transform to ferromagnetic behaviour. The high SAR and saturation temperature observed for 0.8 and 1.0 wt.% nanofluids when placed under higher applied magnetic field of 30 mT and 40 mT can be explained on the basis of above arguments. In order to establish the state of nickel ferrite nanoparticles in the carrier fluid water at different concentrations, ultrasonic investigation was carried out on all prepared nanofluids in the temperature range of 303 to 333 K.

Ultrasonic studies: The behaviour and nature of association of nickel ferrite nanoparticles in the carrier fluid water at varying concentrations (0.2, 0.4, 0.6, 0.8 and 1.0 wt.%) in the temperature range of 303–333 K are investigated by ultrasonic velocity measurements. The ultrasonic wave propagation through nanofluid were measured using single frequency (2 MHz) continuous wave ultrasonic interferometer (Modal VCT-70 A, Mittal Enterprises, India) with an accuracy of $\pm 0.05\%$ of frequency. Ultrasonic waves are altered by a movable metallic plate kept parallel to the quartz plate. If the separation between these plates is exactly a whole multiple of the sound wavelength, standing waves are formed in the nanofluids. The acoustic

resonance gives rise to maximum anode current. The distance between the plates is now increased or decreased, maximum anode current was observed when the variation is half the wavelength or multiple of it. Acoustic parameters such as ultrasonic velocity (V) and acoustic impedance (Z) were calculated using the following equations.

The ultrasonic velocity inside the nanofluids can be determined using the following equation:

$$C = \lambda f$$

where C is the ultrasonic velocity, λ is wavelength of ultrasound inside the nanofluid and f is the frequency of ultrasonic oscillator (2 MHz).

From the values of ultrasonic velocity (C) and density (ρ) of the nanofluids the specific acoustic impedance (Z_i) can be calculated using the formula:

$$Z_i = \frac{\rho_c}{C}$$

Effect of concentration on ultrasonic parameters: The variation of ultrasonic parameters with concentration of nanofluids are shown in Fig. 6a. The ultrasonic velocity of all the nanofluids studied are higher than that of water. At 303 K, the ultrasonic velocity increases with increase of concentration up to 0.8 wt.% and above which it decreases. When the temperature is raised from 303 to 313 K, it was found that the increase in ultrasonic velocity occur only up to 0.6 wt.% beyond which it decreases. At temperatures above 313 K, the ultrasonic velocity increases up to 0.4 wt.%, and then it decreases. The interactions between nickel nanoparticles and the surface of water molecules, which disrupt the hydrogen-bonded open and closed structure of water, and thus improve sound propagation through the nanofluid, are indicated by the initial increase of ultrasonic velocity. On the other hand, decrease in the ultrasonic velocity beyond 0.6 wt.% of nanoparticles concentrations shows there are interactions only between particles and the structure of water (carrier fluid) is not be disturbed which leads to the agglomeration of particles takes place to form small cluster causing additional hindrance for sound propagation. The effect of concentration on acoustic impedance is similar to that of ultrasonic velocity at all temperatures (Fig. 6b). The value of impedance depends on the intermolecular distance between molecules. The intermolecular distance will be large when there are interactions between particle and fluid whereas it will be small if there are interactions between only particles. Generally, high impedance results at higher intermolecular distances. The initial increase of impedance indicate existing of higher intermolecular distances up to 0.6 wt.% nanoparticle concentrations (Fig. 6b), which establishes that nanoparticle is interacting only with carrier fluid there by preventing particle agglomeration and cluster formation. But above 0.6 wt.% concentration impedance found to start decreasing which shows decreasing of intermolecular distances due to the occurrence of particle-particle interactions, which facilitate the particle agglomeration and cluster formation.

Effect of temperature: The variation of ultrasonic velocity with temperature for all the nanofluids are shown in Fig. 7a. In dilute nanofluids (0.2 and 0.4), ultrasonic velocity increases

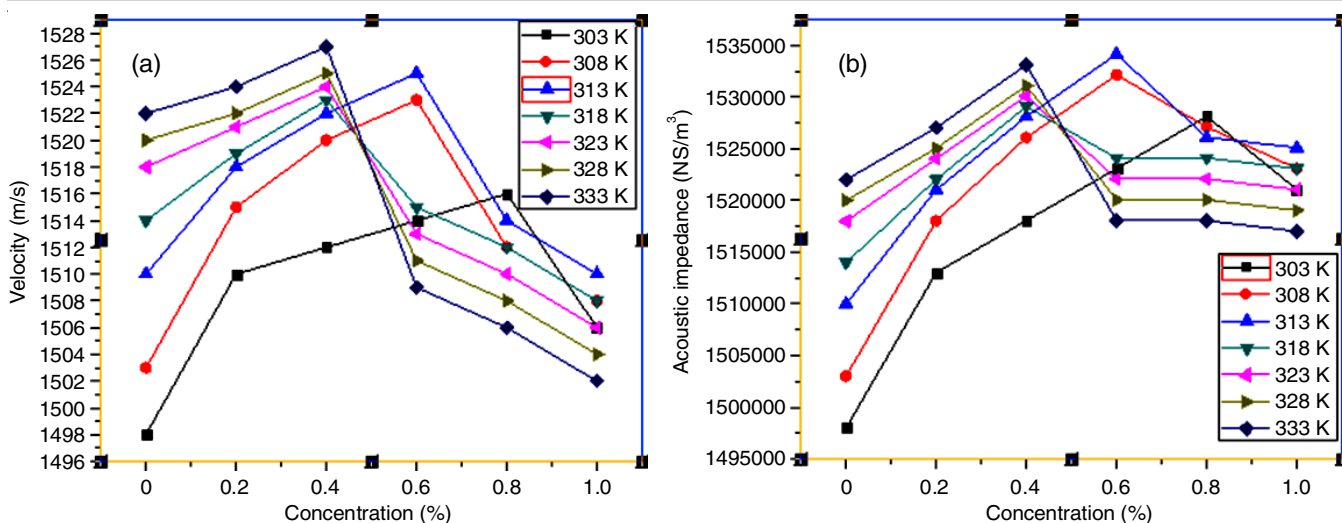


Fig. 6. Variation of (a) ultrasonic velocity and (b) acoustic impedance with concentration

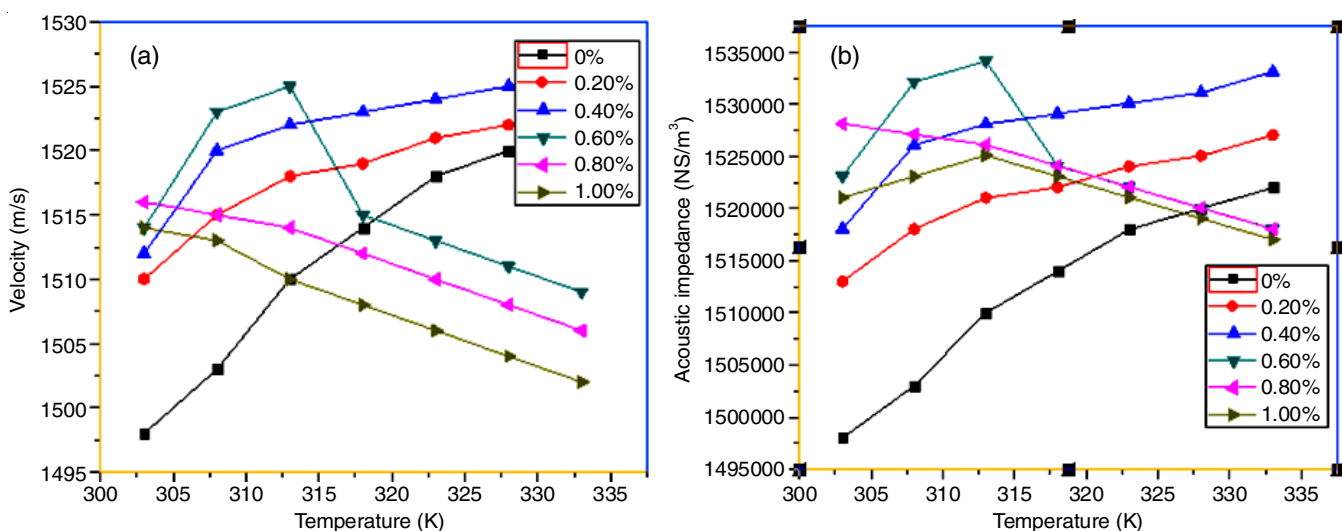


Fig. 7. Variation of (a) ultrasonic velocity and (b) acoustic impedance with temperature

with temperature till 333 K studied in the present investigation. But for 0.6 wt.% sample, it is increasing up to 312 K beyond which the value of ultrasonic velocity decreases. On the other hand, the ultrasonic velocity continues to decrease right from the initial temperature of 303 K for 0.8 and 1.0 wt.% samples. The variation of acoustic impedance also follow the same trend as that of ultrasonic velocity (Fig. 7b).

The state and behaviour of nickel ferrite nanoparticles is well established by the critical analysis of ultrasonic parameters at various concentrations and temperatures as follows:

(i) In nickel nanofluids of concentrations 0.2 and 0.4 wt.%, there are strong interaction between the nanoparticles and fluid molecules at all temperatures studied.

(ii) A sample of 0.6 wt.% exhibit different behaviours at low and high temperatures. When the temperature is less than 312 K particle-fluid interaction prevails but on increasing temperature above 312 K, the particle-particle interaction occurs favouring the agglomeration of nanoparticles.

(iii) In concentrated nanofluids (0.8 and 1.0 wt.%), there are no interactions between particle and fluid molecule at all

temperatures. But particle-particle interaction occurs predominantly at all temperatures resulting in the formation of small cluster.

Conclusion

The nickel ferrite nanoparticles used for the preparation of nanofluids possess superparamagnetic characteristics with an average particle size of 28.44 nm is reported. As the magnetic behaviour of nickel nanoferrite is size sensitive, the superparamagnetic characteristics will be retained only if the particle size is within 30 nm. The hyperthermia studies show that the less concentrated nickel ferrite nanofluids (0.2 and 0.4 wt.%) quickly attain threshold hyperthermia temperature of 43 °C when exposed to lower applied AC magnetic field of range 5 mT to 20 mT. The ultrasonic studies of these samples demonstrate association of nickel nanoparticles with carrier fluid water through cohesive forces mainly hydrogen bonding and keep the particles in an isolated state. It is concluded that at higher concentration, particle-particle interaction predominantly occurs leading to increase in particle size beyond 30 nm, so that the

magnetic characteristics of nickel ferrite nanoparticles may change from superparamagnetic to ferromagnetic nature. In ferromagnetic materials with bigger particle size the Brownian and Neel relaxations do not occur and hence cannot contribute for induction heating. This could be the reason for less SAR and corresponding low saturation temperature observed for 0.8 and 1.0 wt.% samples. However, ferromagnetic materials also possess the induction heating property but generally they require higher AC magnetic field for the transformation of absorbed magnetic power into heat energy through an alternating phenomena of hysteresis loss mechanism. The observed increase of saturation temperature and SAR values with increase of applied magnetic field for 0.8 and 1.0 wt.% samples can be explained by hysteresis loss mechanism of induction heating.

CONFLICT OF INTEREST

The authors declare that there is no conflict of interests regarding the publication of this article.

REFERENCES

- M. Auffan, J. Rose, J.-Y. Bottero, G.V. Lowry, J.-P. Jolivet and M.R. Wiesner, *Nat. Nanotechnol.*, **4**, 634 (2009); <https://doi.org/10.1038/nnano.2009.242>
- X. Gao, Y. Cui, R.M. Levenson, L.W.K. Chung and S. Nie, *Nat. Biotechnol.*, **22**, 969 (2004); <https://doi.org/10.1038/nbt994>
- M.E. Akerman, W.C.W. Chan, P. Laakkonen, S.N. Bhatia and E. Ruoslahti, *Proc. Natl. Acad. Sci. USA*, **99**, 12617 (2002); <https://doi.org/10.1073/pnas.152463399>
- S. Lanone and J. Boczkowski, *Curr. Mol. Med.*, **6**, 651 (2006); <https://doi.org/10.2174/156652406778195026>
- O. Hosu, M. Tertis and C. Cristea, *Magnetochemistry*, **5**, 55 (2019); <https://doi.org/10.3390/magnetochemistry5040055>
- F. Schlachetzki, Y. Zhang, R.J. Boado and W.M. Pardridge, *Neurology*, **62**, 1275 (2004); <https://doi.org/10.1212/01.WNL.0000120551.38463.D9>
- T.M. Allen and P.R. Cullis, *Science*, **303**, 1818 (2004); <https://doi.org/10.1126/science.1095833>
- A.H. Faraji and P. Wipf, *Bioorg. Med. Chem.*, **17**, 2950 (2009); <https://doi.org/10.1016/j.bmc.2009.02.043>
- J. Nicolas, S. Mura, D. Brambilla, N. Mackiewicz and P. Couvreur, *Chem. Soc. Rev.*, **42**, 1147 (2013); <https://doi.org/10.1039/C2CS35265F>
- A.E. John, N.W. Lukacs, A.A. Berlin, A. Palecanda, R.F. Bargatze, L.M. Stoolman and J.O. Nagy, *FASEB J.*, **17**, 2296 (2003); <https://doi.org/10.1096/fj.03-0166fje>
- M. Kumar, X. Kong, A.K. Behera, G.R. Hellermann, R.F. Lockey and S.S. Mohapatra, *Genet. Vaccines Ther.*, **1**, 3 (2003); <https://doi.org/10.1186/1479-0556-1-3>
- F.A. Jaffer and R. Weissleder, *JAMA*, **293**, 855 (2005); <https://doi.org/10.1001/jama.293.7.855>
- D.L. Thorek, A.K. Chen, J. Czupryna and A. Tsourkas, *Ann. Biomed. Eng.*, **34**, 23 (2006); <https://doi.org/10.1007/s10439-005-9002-7>
- H. Lee, E. Lee, D.K. Kim, N.K. Jang, Y.Y. Jeong and S. Jon, *J. Am. Chem. Soc.*, **128**, 7383 (2006); <https://doi.org/10.1021/ja061529k>
- T.V. Sreekumar, A. Das, L. Chandra, A. Srivastava and B.K.U. Rao, *J. Biomed. Nanotechnol.*, **5**, 115 (2009); <https://doi.org/10.1166/jbn.2009.040>
- K.D. Miller, R.L. Siegel, C.C. Lin, A.B. Mariotto, J.L. Kramer, J.H. Rowland, K.D. Stein, R. Alteri and A. Jemal, *CA Cancer J. Clin.*, **66**, 271 (2016); <https://doi.org/10.3322/caac.21349>
- Y. Du, L. Xia, A. Jo, R.M. Davis, P. Bissel, M.F. Ehrich and D.G.I. Kingston, *Bioconjug. Chem.*, **29**, 420 (2018); <https://doi.org/10.1021/acs.bioconjchem.7b00756>
- S. Kalimuthu, P. Gangadaran, R.L. Rajendran, L. Zhu, J.M. Oh, H.W. Lee, A. Gopal, S.H. Baek, S.Y. Jeong, S.-W. Lee, J. Lee and B.-C. Ahn, *Front. Pharmacol.*, **9**, 1116 (2018); <https://doi.org/10.3389/fphar.2018.01116>
- V.V. Gwenin, C.D. Gwenin and M. Kalaji, *Langmuir*, **27**, 14300 (2011); <https://doi.org/10.1021/la202951p>
- I.M. Obaidat, B. Issa and Y. Haik, *Nanomaterials*, **5**, 63 (2015); <https://doi.org/10.3390/nano5010063>
- E. Ahilandeswari, R. Rajesh Kanna and K. Sakthipandi, *Physica B*, **599**, 412425 (2020); <https://doi.org/10.1016/j.physb.2020.412425>
- G. Rana, P. Dhiman, A. Kumar, D.-V.N. Vo, G. Sharma, S. Sharma and M. Naushad, *Chem. Eng. Res. Des.*, **175**, 182 (2021); <https://doi.org/10.1016/j.cherd.2021.08.040>
- P. Caetano, N. Simões, P. Pinto, L. Fernandez-Outon, A. Albuquerque, W. Macedo and J. Ardisson, *J. Braz. Chem. Soc.*, **31**, 2452 (2020); <https://doi.org/10.21577/0103-5053.20200120>
- K. Nejati and R. Zabihi, *Chem. Cent. J.*, **6**, 23 (2012); <https://doi.org/10.1186/1752-153X-6-23>
- S. Bae, S.W. Lee and Y. Takemura, *Appl. Phys. Lett.*, **89**, 252503 (2006); <https://doi.org/10.1063/1.2420769>
- M. Nabeel Rashin and J. Hemalatha, *Ultrasonics*, **52**, 1024 (2012); <https://doi.org/10.1016/j.ultras.2012.08.005>
- S. Chakraborty, J. Mukherjee, M. Manna, P. Ghosh, S. Das and M.B. Denys, *Ultrason. Sonochem.*, **19**, 1044 (2012); <https://doi.org/10.1016/j.ultsonch.2012.01.016>
- I. Hilger, K. Fruhauf, W. Andra, R. Hiergeist, R. Hergt and W.A. Kaiser, *Acad. Radiol.*, **9**, 198 (2002); [https://doi.org/10.1016/S1076-6332\(03\)80171-X](https://doi.org/10.1016/S1076-6332(03)80171-X)
- N.J. Jebarathinam, M. Eswaramoorthy and V. Krishnasamy, *Bull. Chem. Soc. Jpn.*, **67**, 3334 (1994); <https://doi.org/10.1246/bcsj.67.3334>
- Y.C. Wang, J. Ding, J.H. Yin, B.H. Liu, J.B. Yi and S. Yu, *J. Appl. Phys.*, **98**, 124306 (2005); <https://doi.org/10.1063/1.2148632>
- A. Lassoued, M.S. Lassoued, B. Dkhil, S. Ammar and A. Gadri, *Physica E*, **101**, 212 (2018); <https://doi.org/10.1016/j.physe.2018.04.009>
- X. Wang, X. Xu and S.U.S. Choi, *J. Thermophys. Heat Trans.*, **13**, 474 (1999); <https://doi.org/10.2514/2.6486>
- E.L. Verde, G.T. Landi, M.S. Carrião, A.L. Drummond, J.A. Gomes, E.D. Vieira, M.H. Sousa and A.F. Bakuzis, *AIP Adv.*, **2**, 032120 (2012); <https://doi.org/10.1063/1.4739533>
- S. Larumbe, J.I. Pérez-Landazábal, J.M. Pastor and C. Gómez-Polo, *J. Appl. Phys.*, **111**, 103911 (2012); <https://doi.org/10.1063/1.4720079>